Inorganic Chemistry

Article

pubs.acs.org/IC

Structural Plasticity: How Intermetallics Deform Themselves in Response to Chemical Pressure, and the Complex Structures That Result

Veronica M. Berns and Daniel C. Fredrickson*

Department of Chemistry, University of Wisconsin−Madison, 1101 University Avenue, Madison, Wisconsin 53706, United States

Supporting Information

ABSTRACT: Interfaces between periodic domains play a crucial role in the properties of metallic materials, as is vividly illustrated by the way in which the familiar malleability of many metals arises from the formation and migration of dislocations. In complex intermetallics, such interfaces can occur as an integral part of the ground-state crystal structure, rather than as defects, resulting in such marvels as the $NaCd_2$ structure (whose giant cubic unit cell contains more than 1000 atoms). However, the sources of the periodic interfaces in intermetallics remain mysterious, unlike the dislocations in simple metals, which can be associated with the exertion of physical stresses. In this Article, we propose and explore the concept of structural plasticity, the hypothesis that interfaces in complex intermetallic structures similarly result from stresses, but ones that are inherent in a defect-free parent structure, rather than being externally applied. Using DFT-chemical pressure analysis, we show how the complex structures of Ca_2Ag_7 (Yb_2Ag_7 type), $Ca_{14}Cd_{51}$ ($Gd_{14}Ag_{51}$ type), and the 1/1 Tsai-type quasicrystal approximant $CaCd_6$ (YCd_6 type) can all be traced to large negative pressures around the Ca atoms of a common progenitor structure, the $CaCu_5$ type with its simple hexagonal 6-atom unit cell. Two structural paths are found by which the compounds provide relief to the Ca atoms' negative pressures: a Ca-rich pathway, where lower coordination numbers are achieved through defects eliminating transition metal (TM) atoms from the structure; and a TM-rich path, along which the addition of spacer Cd atoms provides the Ca coordination environments greater independence from each other as they contract. The common origins of these structures in the presence of stresses within a single parent structure highlights the diverse paths by which intermetallics can cope with competing interactions, and the role that structural plasticity may play in navigating this diversity.

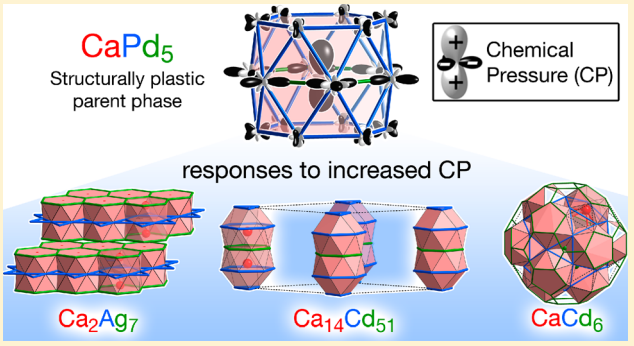

1. INTRODUCTION

The development of materials properties is a multiscale endeavor, as the physical behavior of a material depends not only on the bulk crystal structures of its component compounds, but also on the character and distribution of the interfaces within and between them. A classic example is the plasticity of malleable metals, which arises from the ease with which dislocations can form and migrate in response to physical stresses.[1] More recently, nanostructuring has been used to introduce interfaces to enhance the mechanical,[2,3] thermoelectric,[4−9] and optical properties[10,11] over the bulk phases alone. Techniques to control interface formation thus valuably complement the search for new solid state compounds with useful properties.

An important opportunity is offered by intermetallic phases, as they represent a class of compounds in which interfaces can occur periodically as intrinsic aspects of their crystal structures. For instance, domains of the simple Laves phase crystal structures can be perceived in the structures of Fe_7W_6 (the μ-phase, $hR13$),[12] α-Mn ($cI58$),[13] γ-brass ($cI52$),[14] $Zr_{21}Re_{25}$ ($hR92$),[15] and $NaCd_2$ ($cF1176$).[13,16] However, whereas metastable interfaces in other materials can be created through mechanical deformation or the synthetic targeting of nanostructures, the role of interfaces in stabilizing intermetallics remains an open question, one whose answer may offer ways to tune crystal structures for particular applications.

In this Article, we will offer an approach to understanding the origins of interfaces in intermetallics based on their structural similarities to dislocations in malleable metals. The association of dislocations with stress led us to wonder whether the fragmentation of simple intermetallic structures to yield more intricate ones may be indicative of another kind of force: one arising internally within a simple structure. The interfaces between simple structures in complex intermetallics would then represent the ability of a crystal structure to deform itself in response to internal tension, an effect we term structural plasticity. Structural plasticity, then, is a hypothesis that solid-state phases can respond to stresses inherent in them in a manner analogous to their reactions to stresses applied

Received: August 21, 2014
Published: September 19, 2014

   dx.doi.org/10.1021/ic5020412 | Inorg. Chem. 2014, 53, 10762−10771

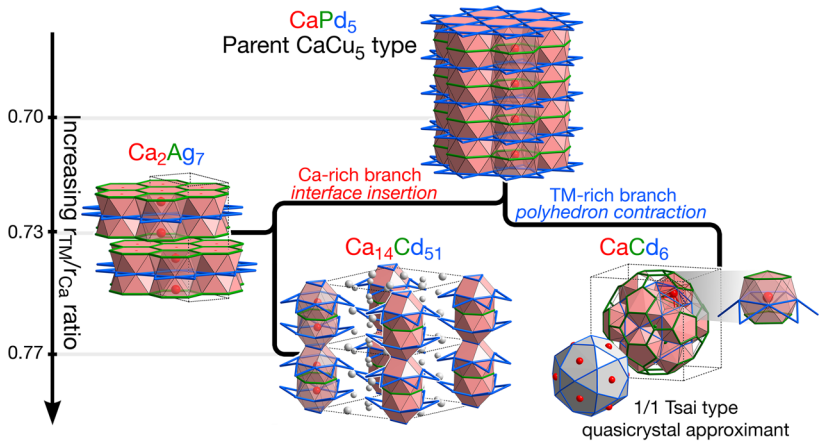

Figure 1. Structural plasticity of the $CaCu_5$ structure type. As the transition metal (TM) to Ca radius ratio increases, the simple $CaCu_5$ type fragments into more complex structures.

externally, with one important difference: the result of the process is a new and more complex crystal structure (which retains fragments of the original), rather than a macroscopically deformed object.

With the advent of our recently developed DFT-chemical pressure (CP) analysis,[17−19] we have begun to see that the requisite internal stresses necessary for structural plasticity are a frequent occurrence in simple intermetallic structures.[17−23] Examples of simple structure types found to exhibit such local pressures include the $CaCu_5$,[17,24] W_5Si_3,[18] and $AuCu_3$ types.[23] For some combinations of elements, these pressures can be so severe that they drive structural transformations, such as the insertion of interfaces in the first two instances (as expected from the analogy with dislocations), and the incorporation of guest atoms in the third case.

Over the course of this Article, we will use the DFT-CP approach—combining results on new systems and updates on our earlier analyses with the latest CP methods—to explore how far this concept can be taken in explaining the range of crystal structures encountered in intermetallic systems. Focusing on one simple structure type as a model system, the $CaCu_5$ type, we will show how the various degrees of chemical pressure can give rise to a progression of crystal structures (Figure 1). The $CaCu_5$ type will emerge here as the progenitor to three more complex structures: Ca_2Ag_7 (Yb_2Ag_7 type),[25−27] the $Ca_{14}Cd_{51}$ ($Gd_{14}Ag_{51}$ type),[28,29] and the 1/1 Tsai-type quasicrystal approximant $CaCd_6$ (YCd_6 type).[30,31]

Two distinct structural paths will become apparent for the release of negative pressures at the Ca atoms: One may be called the Ca-rich branch and is characterized by the deletion of transition metal atoms, which lowers the dimensionality of the $CaCu_5$-type features to slabs (Ca_2Ag_7) and columns ($Ca_{14}Cd_{51}$). The second path, the transition metal (TM)-rich branch, involves the insertion rather than the deletion of TM atoms, and ultimately supports the creation of the curvature underlying the icosahedral clusters of the Tsai-type approximant. The resulting "family tree" of structures illustrates the potential of the structural plasticity concept to describe and relate intermetallic crystal structures in terms that reflect the driving forces shaping them, and offer suggestions for synthetic experiments aimed at modulating these driving forces.

2. EXPERIMENTAL SECTION

The DFT-chemical pressure (CP) analysis was applied to the results of LDA-DFT calculations on a variety of $CaCu_5$-type phases, Ca_2Ag_7 and Ca_2Cd_7 in the Yb_2Ag_7 type, and ordered models of $Ca_{14}Cd_{51}$ and $CaCd_6$. The LDA-DFT calculations were performed with ABINIT,[32,33] using plane-wave basis sets. All calculations in ABINIT utilized the LDA exchange-correlation functional of Goedecker, Teter, and Hutter[34] and Hartswigen−Goedecker−Hutter norm-conserving pseudopotentials.[35] Further computational details, such as the *k*-point grids and energy cutoffs used for each calculation, are provided in the Supporting Information.

All crystal structures were geometrically optimized with ABINIT using a two-step procedure: the ion positions were first relaxed within a fixed unit cell, after which all parameters were simultaneously optimized. Single-point calculations were then performed at the geometrically optimized volume, and a slightly reduced and expanded volumes (total volume range = 3%). From these calculations, grid data for the kinetic energy densities, electronic densities, and local components of the Kohn−Sham potential were extracted as input for the DFT-CP analysis.

The CP analysis itself is carried out using the latest version of our DFT-CP package,[36] which consists of two main programs: *CPmap*, and *CPintegrate*. *CPmap* utilizes the spatially resolved energy outputs from the single-point calculations to create a pressure map of the entire unit cell, and employs the grid unwarping procedure.[19] *CPintegrate* interprets the map through integrating the pressures within the regions assigned to each interatomic contact and projecting the results onto spherical harmonics.

Contact volumes were created using the Hirshfeld-inspired scheme, in which the radial free atom electron density profiles placed at each of the atomic positions is used to determine which two atoms contribute most strongly to the pressure at each voxel.[19] For the compounds examined here, this scheme on its own led to a strong sensitivity of the results to changes in the profiles used, due to the small size of the atomic core regions and the tendency for them to be dominated by a single interaction type. This sensitivity was remedied through the use of isotropic core averaging.[18] In this procedure, the spherical symmetric portions of the pressure map around the atomic positions within a specified radius are replaced with their average values, while the directional aspects of the pressure map are left unchanged. The program *CPisocore* newly added to our DFT-CP package applies this averaging between the *CPmap* and *CPintegrate* steps. For the results presented here sphere radii for the procedure were set to 85% of the standard metallic radii of the elements, while making sure that no overlap between the spheres occurred.

dx.doi.org/10.1021/ic5020412 | *Inorg. Chem.* 2014, 53, 10762−10771

3. RESULTS AND DISCUSSION

3.1. Chemical Pressure in $CaCu_5$-Type Compounds. As we will see over the course of this Article, an opportunity for the emergence of structural plasticity is found in the $CaCu_5$ structure type, whose simple structure belies a tense compromise between competing interactions. The $CaCu_5$ type can be viewed in terms of a stacking of hexagonal layers (Figure 2a), in which kagome (blue) and honeycomb (green) nets of transition metal atoms alternate. Atoms of a second, relatively electropositive element (red), such as an alkaline earth or lanthanide, lie in the hexagonal void spaces that arise from this layer stacking. The result is described by a simple hexagonal unit cell containing only six atoms.

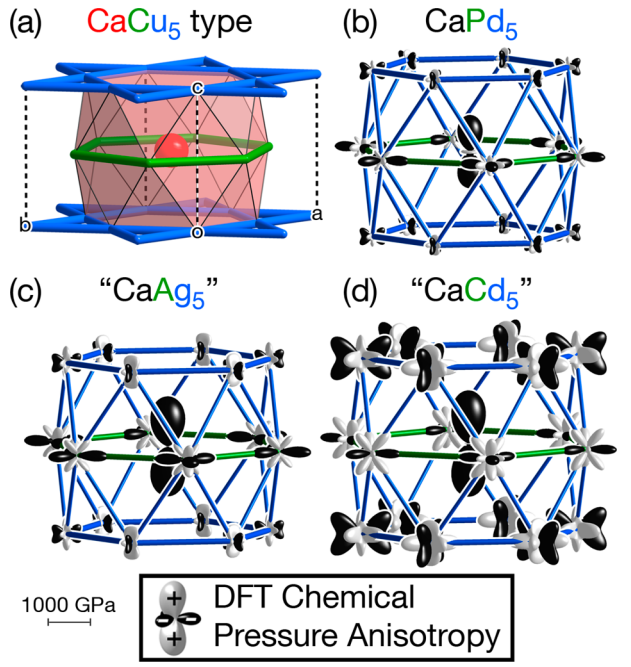

Figure 2. Chemical pressure (CP) schemes for $CaCu_5$ type phases. (a) The crystal structure is comprised of alternating layers of transition metal kagome (blue) and honeycomb (green) nets. The honeycomb nets contain a calcium stuffing atom in each hexagonal ring. CP distributions are plotted for $CaCu_5$-type phases with the compositions (b) $CaPd_5$, (c) $CaAg_5$, and (d) $CaCd_5$. Of these, $CaPd_5$ is the only observed compound, while the other two are hypothetical. *Plotting conventions:* the distance of the CP surfaces from the atomic centers is proportional to the sum of the voxel pressures along that direction (see scale bar), while the sign of the pressure is given by the color of the surface (black for negative, white for positive).

It is in this simplicity, however, that the possibility of internal strain arises: all of the atoms lie on high-symmetry positions, and the only parameters that can be adjusted to optimize the various Ca−Ag, Ca−Ca, and Ag−Ag interatomic distances are the cell volume and c/a ratio. Clearly the structure type is not flexible enough to simultaneously achieve ideal distances for all interaction types. Instead, the experimentally observed distances must reflect some sort of compromise, as has been recognized from empirical factors for a wide range of intermetallics in the insightful work of W. B. Pearson.[37]

The opportunity to visualize such compromises through quantum mechanical calculations is offered by the DFT-Chemical Pressure (CP) method. In this technique, the macroscopic pressure of a phase is resolved onto a pressure grid passing through its crystal structure. This pressure grid can then be interpreted in terms of interatomic interactions, through the integration and projection of pressures within volumes corresponding to specific contacts between atoms.

In Figure 2b−d, we present the CP schemes obtained in this manner for three $CaCu_5$-type phases, one experimentally observed ($CaPd_5$) and two that are hypothetical ($CaAg_5$ and $CaCd_5$) according to the phase diagrams.[29,38,39] Here, the distributions of pressures around the atoms are represented with surfaces centered on the nuclear positions. The distance from an atomic center to a point on its CP surface represents the magnitude of the pressures experienced along that direction (in terms of the product of the number of voxels within the contact volume and their average pressure value), whereas the color of the surface represents the sign of the pressure. Black indicates negative pressures calling for the contraction of the structure, while white is used to label positive pressures which push for the expansion of the structure (this color scheme can be made intuitive by reference to astronomy: black holes pull their surroundings toward them, while stars appear white because of the light that they radiate).

The result for the first compound, $CaPd_5$, exhibits several features common to all three. The Ca atom at the center of the plot appears with a large CP surface resembling a d_{z^2} orbital: large black lobes dominate along the vertical direction (corresponding to a pressure value of −902 GPa at the apexes),[40] whereas a small donut of white runs along the equator. The negative pressure lobes correspond to Ca−Pd distances that are longer than ideal for the palladium on the kagome nets above and below (blue), while the positive pressures of the ring indicate that the Ca−Pd contacts in the plane are already too short. Between the Pd atoms, the pressure features appear smaller, with the shorter contacts in blue exhibiting small positive pressures, and negative pressures occurring along the longer contacts on the honeycomb layer (green). These positive and negative CP features balance out so that the net pressure on the phase is zero.

This balance changes when we substitute Pd with Ag or Cd.[41] Replacing Pd with larger atoms leads to an expansion of the transition metal sublattice, including the hexagonal voids in which the Ca atoms lie. The chemical pressure scheme of $CaAg_5$ reflects this, with the donuts of positive pressure around the Ca atom largely vanishing, as the in-plane Ca−Ag contacts become relatively less short. In its place positive pressure features grow more pronounced between the Ag atoms. By the time we reach $CaCd_5$, the major tension is between the overly stretched out-of-plane Ca−Cd distances and the contacts within the Cd sublattice that are already too short.

From this perspective, we can rationalize why $CaPd_5$ is an experimentally observed compound, while for $CaAg_5$ and $CaCd_5$ no such $CaCu_5$-type phase exists. In $CaPd_5$, the Ca experiences an awkward fit in its coordination environment, with some neighbors being too close and some too distant. However, this compromise chiefly involves optimizing the heteroatomic interactions which drive the formation of the intermetallic phase. As we move to $CaAg_5$ and $CaCd_5$, the situation shifts more and more toward the formation of optimal heteratomic Ca-TM contacts being impeded by repulsion between the TM atoms. By $CaCd_5$, the Ca atom is becoming simply too small for its coordination environment. As we will see soon, the presence of such internal stresses in the hypothetical $CaAg_5$ and $CaCd_5$ phases sets the stage for structural plasticity.

dx.doi.org/10.1021/ic5020412 | Inorg. Chem. 2014, 53, 10762−10771

3.2. Structural Plasticity in the Ca−Ag System. Having explored the CP distributions within the $CaCu_5$ type, we are now ready to delve into how these internal stresses are relieved by going to more complex structures. Upon moving to these new structures, the compositions will change relative to the original 1:5 composition, which will make direct comparisons of thermodynamic stability difficult. However, we will see that by thinking about the local coordination environments as open systems, from which atoms can come and go, we will be able to explain many of the structural features of these intermetallic phases from the point of view of CP relief.

Let us begin with the closest observed relative to a $CaCu_5$-type in the Ca−Ag system: the Yb_2Ag_7-type Ca_2Ag_7. As is shown in Figure 3, the structure is built from a layering of TM

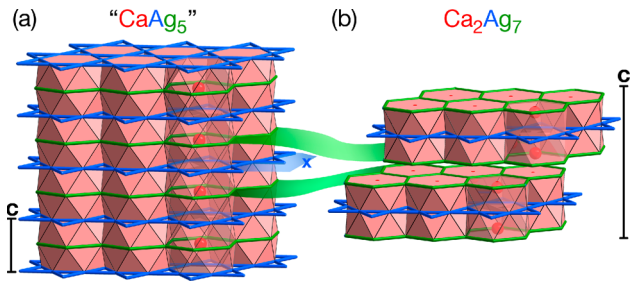

Figure 3. Structural relationship between (a) the $CaCu_5$ type and (b) the crystal structure of Ca_2Ag_7.

honeycomb and kagome nets, with the Ca atoms placed in the hexagons of the honeycomb nets, just as in the $CaCu_5$ type. However, the overall architecture is different: whereas the $CaCu_5$ type exhibits a simple alternation between honeycomb and kagome nets, in Ca_2Ag_7 every other kagome net is missing. These deletions divide the structure into $CaCu_5$-type slabs, which are shifted relative to each other at the interfaces.

Some of the structural characteristics of Ca_2Ag_7 are anticipated by the DFT-CP scheme that we saw earlier for the hypothetical $CaAg_5$ phase (Figure 2c). The dominant features in the $CaAg_5$ CP plot are the presence of large negative pressure lobes pointing up and down from the Ca atom (−1302 GPa at the apexes), which express a strong drive for shorter contacts to the Ag atoms in the layers above and below. The desire of either one of these lobes could be satisfied by the vertical motion of the Ca atom toward either of these layers, but this would solve only half of the issue. Moving the Ca atom up would create shorter Ca−Ag contacts to the layer above, but only at the expense of stretching the already too long contacts to the layer below, while the reverse situation would occur for moving the Ca atom down. In other words, the symmetry-equivalence of the negative pressure lobes leads to a stalemate.

The stalemate ends, however, if a superstructure is created that breaks the symmetry relating the upper and lower Ag layers. This is what is accomplished by the layer-deletions that lead to the Ca_2Ag_7 structure (Figure 4, right). The removal of one kagome layer allows for the Ca atom to move toward the remaining layer and achieve closer Ca−Ag contacts. The motion is further supported by the horizontal shift that occurs between the $CaCu_5$-type slabs as the structure heals. The shift places two Ag atoms from the neighboring layer almost directly above each Ca atom at a distance of 3.14 Å (in our geometrically optimized structure) vs 3.56 Å for the interlayer Ca−Ag contact in $CaAg_5$.

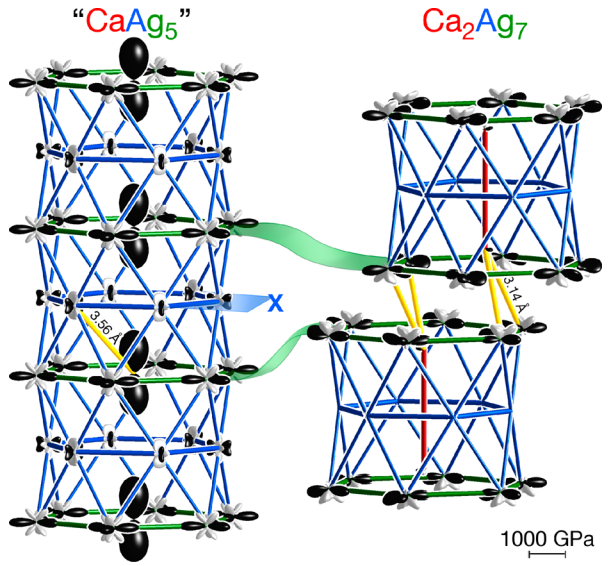

Figure 4. Chemical pressure release on moving from the hypothetical $CaCu_5$-type $CaAg_5$ phase to the observed Ca_2Ag_7 structure. See the caption to Figure 2 for plotting conventions.

These trends in the coordination number and distances mirror our experience with pressure-induced phase transitions. Transitions driven by the application of physical pressure generally lead to an increase in the atoms' coordination numbers. The increased number of neighbors means that each individual interaction is weaker, and this results in a counterintuitive lengthening of bond distances under pressure, a observation known as the pressure−distance paradox.[42] The opposite trend is seen on going from a high pressure phase to a low pressure one: atoms will then take on fewer neighbors at shorter distances. Such a situation occurs as the Ca_2Ag_7 structure forms in response to negative pressures in the Ca environment of the $CaCu_5$ type: the calcium atoms decrease their Ag neighbor count from 18 at an average distance of 3.42 Å to 14 with an average distance of 3.20 Å.

The favorability of this new arrangement is evident in the CP features calculated for Ca_2Ag_7 (Figure 4). On the Ca atoms, the large negative pressure lobes have become substantially reduced, so much so that they are no longer the most prominent CP features. The locus of the stresses is now at the interfaces between $CaCu_5$-type slabs, where positive CP lobes point along interlayer Ag−Ag contacts. The combination of these positive Ag−Ag pressures and residual negative pressures on the Ca atoms suggests that the Ca_2Ag_7 structure is not a universal solution to the CP scheme of the $CaCu_5$ type. Increasing the size of the TM atoms relative to the Ca ones would again begin to stretch the Ca-TM distances. Indeed on moving from the Ca−Ag to Ca−Cd system, more impressive structural transformations are observed, as we will describe in the next section.

3.3. Manifestations of Structural Plasticity in the Ca−Cd System. From the similarities encountered in the CP schemes calculated for the $CaAg_5$ and $CaCd_5$ in the $CaCu_5$ type, it is not surprising the Ca−Cd system would also seek alternatives to this simple structure. What is striking, however, is the number of solutions that the Ca−Cd system finds. At least four Ca−Cd phases exist near the 1:5 composition, which comprise all of the known compounds on the Cd-rich side of the phase diagram between $CaCd_2$ and elemental Cd:

dx.doi.org/10.1021/ic5020412 | Inorg. Chem. 2014, 53, 10762−10771

$Ca_{14}Cd_{51}$,[29,39] $CaCd_{5.7}$,[43] $Ca_{13}Cd_{76}$,[44] and $CaCd_6$.[31] The first of these represents a continuation of the fragmentation of the $CaCu_5$ type seen in Ca_2Ag_7, while the latter three correspond to a Tsai-type icosahedral quasicrystal and its two periodic approximants. Through CP analysis on $Ca_{14}Cd_{51}$ and the simplest Tsai-type approximant, $CaCd_6$, we will see how these phases are also expressions of the simple $CaCu_5$ type's structural plasticity.

3.4. Structural Plasticity-Inspired View of $Ca_{14}Cd_{51}$'s Structure. We begin with $Ca_{14}Cd_{51}$, as it shares common themes with the Ca_2Ag_7 structure we examined above. One simple yet crucial contribution that the theme of structural plasticity can make to our understanding of this compound is to provide a framework for describing its crystal structure. $Ca_{14}Cd_{51}$ crystallizes in the $Gd_{14}Ag_{51}$ structure type (Figure 5) observed in a number of RE-Cu and RE-Ag systems (RE =

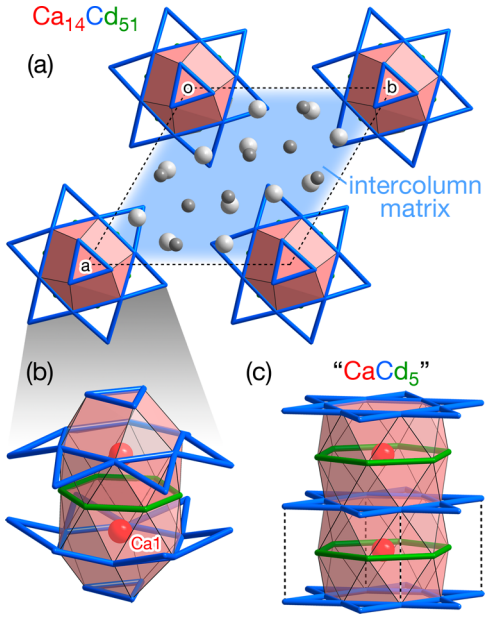

Figure 5. Columns of the $CaCu_5$-type features in the crystal structure of $Ca_{14}Cd_{51}$. (a) The distribution of columns within the unit cell of $Ca_{14}Cd_{51}$. (b) One repeat length of the column, shown alongside (c) the original $CaCu_5$ type.

electropositive metal, such as a lanthanide, actinide, and alkaline earth),[28,45−56] and ternary variants incorporating Ga or Sn.[57−60] This structure's moderately large hexagonal unit cell of 65 atoms is difficult to reduce to a handful of intuitive structural motifs. However, its proximity in composition to a hypothetical $CaCu_5$-type phase encourages us to seek connections to this simpler structure type.

Such a connection becomes immediately apparent upon looking at the coordination environments of the Ca1 sites, which lie along high-symmetry hexagonal axes of the structure (Figure 5a). The Ca1 atoms occur in pairs that lie in spaces created by the stacking of three Cd hexagons, the top and bottom of which can be extended through inclusion of neighboring Cd atoms to make larger fragments of kagome nets (blue). These hexagonal features resemble the hexagonal channels hosting the Ca atoms in the $CaCu_5$ type (Figure 5c). Here, though, the stack is only three hexagons tall, and is terminated on the top and bottom by Cd triangles disordered over two orientations in the refined crystal structure due to their position on a C_6 axis[50] (though in Ca−Hg and Sr−Hg analogues ordered versions have been observed).[61] These $CaCu_5$-type units occur periodically along *c*, separated by shared triangles.

The remainder of the structure could then be conveniently described as a matrix of atoms separating these $CaCu_5$-derived columns from each other (Figure 5a). However, a deeper analysis, involving an admittedly obsessive level of detail, reveals that the coordination environments of the Ca atoms in this region (Ca2 and Ca3) can be similarly interpreted in terms of CP release (readers not interested in the specifics are welcome to rejoin us at the beginning of section 3.5). For both Ca2 and Ca3, the Ca atoms appear in pairs whose nearest neighbors can be sorted into three nearly planar, distorted rings by analogy to the three hexagons of the Ca coordination polyhedra in the $CaCu_5$ type (Figure 6a, b).

Although these rings exhibit severe deviations away from those of the $CaCu_5$ type, these discrepancies are in-line with the expectations of the CP analysis. The upper and lower rings are contracted relative to a hexagon, while the central ring remains either hexagonal (Ca3) or is expanded to a bent heptagon (Ca2). This appears to be excellent tailoring of a Ca coordination environment that originally exhibited negative pressure lobes pointing up and down, and a small but positive pressure ring in the horizontal plane.

Now that we have rationalized the shapes of these irregular coordination polyhedra, we are now faced with seeing how they are arranged in the matrix space between Ca1 columns. The polyhedra surrounding the Ca2 and Ca3 dimers have a dumbbell-like shape (Figures 6a, b), which allow them to pack efficiently in a triangular fashion such that the head of each dimer lies in the neck of another (Figure 6c, d). This packing is supported by an arrangement of square and triangular faces around the perimeters of the dumbbells that is complementary between head and neck. The compatibility is such that the triangular units seamlessly fuse through the sharing of these faces (Figure 6e, f). Through similar face-sharing the Ca2 and Ca3 triangular units join into sheets with openings for the Ca1 columns to pass through (Figure 6g−j).

The Ca2 and Ca3 sheets stack in an alternating fashion along the *c*-axis, with the dimer orientations shifting by almost 90° between neighboring sheets (Figure 6k). The staggering of the dimer orientations allows the neighboring dimers to nestle closely neck-to-neck (Figure 6l), and share faces (as can be seen in more detail in the Supporting Information).

In this discussion of the Ca coordination environments of $Ca_{14}Cd_{51}$, we have accounted for all of the symmetry-distinct sites of the crystal structure. All atoms in the structure participate in the $CaCu_5$-derived columns surrounding the Ca1 sites, and/or the irregular polyhedra of the Ca2 and Ca3 sites, whose shapes seem adapted to respond to the chemical pressures experienced by the Ca atoms in the $CaCu_5$ type. In this way, the full structure can be expressed as providing a favorable alternative to the constrained geometry of the $CaCu_5$ type.

3.5. Chemical Pressure Release in $Ca_{14}Cd_{51}$. How well do the structural features we just described for $Ca_{14}Cd_{51}$ really provide relief to the CP issues that a $CaCu_5$-type $CaCd_5$ phase would experience? In Figure 7, we follow the CP distributions around the Ca atoms in Ca−Cd phase as the $CaCu_5$ type is broken up through the insertion of interfaces. For the $CaCu_5$-type $CaCd_5$ (Figure 7a), we see the familiar large negative pressures lobes on the Ca atoms (reaching −1253 GPa along

dx.doi.org/10.1021/ic5020412 | Inorg. Chem. 2014, 53, 10762−10771

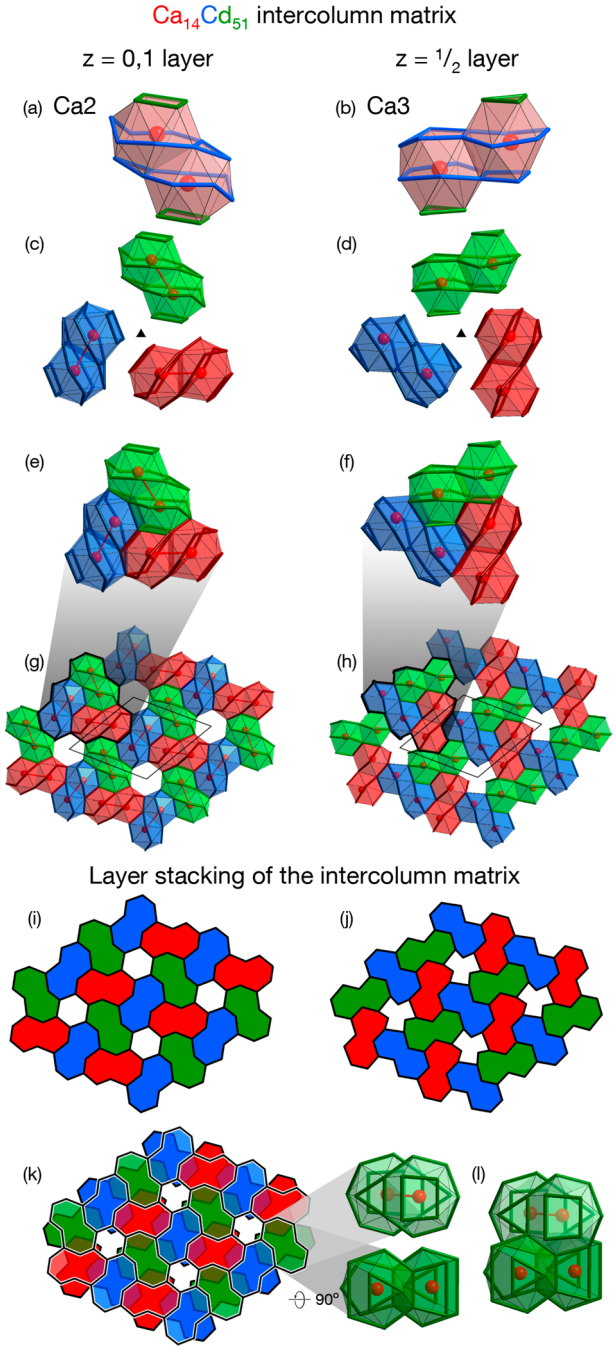

Figure 6. Structure of the intercolumnar matrix in $Ca_{14}Cd_{51}$. (a, b) Coordination environments of the Ca2 and Ca3 sites occur as dumbbell-shaped homodimers. (c, d) Dumbbells pack neatly into triangular units in a head-to-neck fashion, which is supported by (e, f) the sharing of complementary faces. (g, h) Triangular units in turn fuse with each other into sheets, which are represented schematically in (i, j). (k) Ca2 and Ca3 layers stack in an alternating fashion along *c* with neighboring dumbbells staggered to allow (l) the sharing of atoms at neck-to-neck contacts.

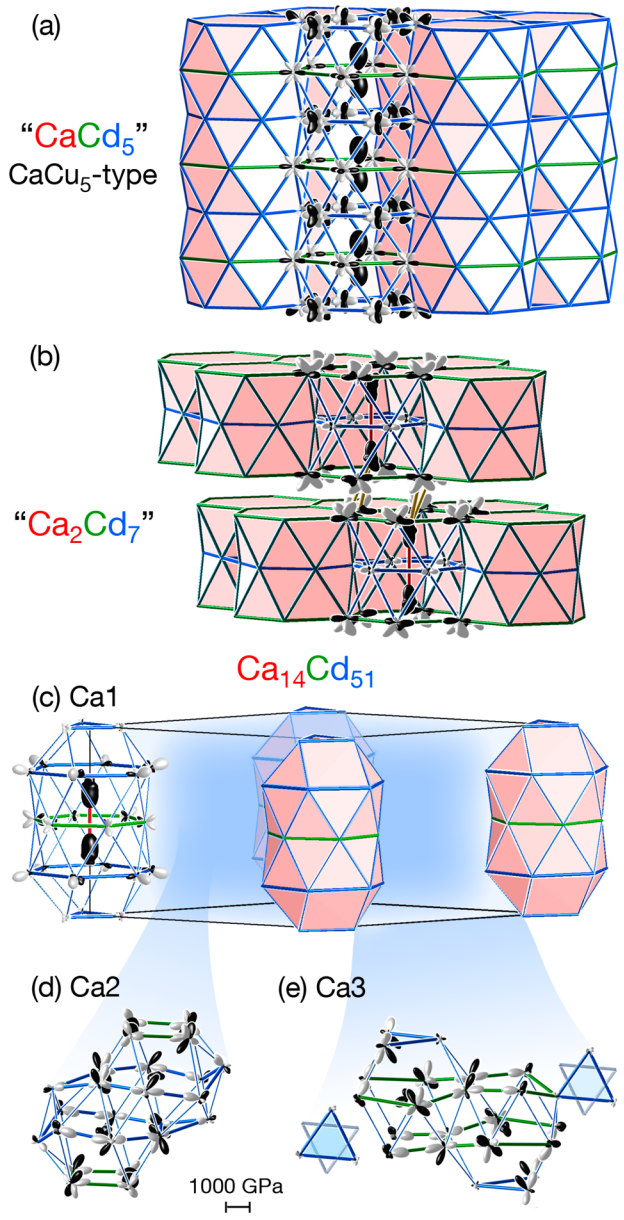

Figure 7. Progression in the chemical pressure scheme as the (a) hypothetical $CaCu_5$-type $CaCd_5$ phase is fragmented first to (b) a Ca_2Ag_7-type Ca_2Cd_7 phase (also hypothetical), and then to (c–e) the observed $Gd_{14}Ag_{51}$-type $Ca_{14}Cd_{51}$ phase. Plotting conventions are given in the caption to Figure 2.

the *z* axis) balanced against positive pressures within the Cd sublattice.

Introducing planar interfaces to form a Cd analog to Ca_2Ag_7 would seem to be a reasonable solution to this tension. In fact, CP calculations on such a structure (Figure 7b) show a similar form of relief around the Ca sites as was found earlier for Ca_2Ag_7, with the most intense negative CP lobes on the Ca now only corresponding to −886 GPa. Unlike in Ca_2Ag_7, however, the Ca atoms exhibit prominent negative CP features pointing across the interface (reaching −622 GPa), which are countered by positive lobes on the interfacial Cd atoms. Even with the presence of these interfaces, the Cd atoms are sufficiently large that bonding around the Ca atoms is still impeded.

Moving to the $Ca_{14}Cd_{51}$ structure, with its more extensive fragmentation of the $CaCu_5$ type, leads are a larger release of the Ca atoms' negative CP (Figure 7c–e). As in Ca_2Cd_7, the CP distributions around the Ca sites appear much more isotropic than in the $CaCu_5$ type. For the majority Ca2 and Ca3 sites achieve negative CPs as mild as −390 and −630 GPa along their most intense directions (mild, that is, relative to the corresponding value of −1253 GPa for the $CaCu_5$ type). The

dx.doi.org/10.1021/ic5020412 | *Inorg. Chem.* 2014, 53, 10762–10771

Ca1 sites in the $CaCu_5$-derived columns bear CP lobes of −1158 GPa toward the center of the $CaCu_5$-type unit and −250 GPa toward the triangles at the kinks in the column. The relatively large value of the former may indicate that the Ca1-centered columns are templated by the geometrical requirements of intercolumnar matrix, rather than vice versa.

In addition to illustrating a driving force for the formation of the phase, the CP schemes of the Ca2 and Ca3 coordination environments help provide a retrospective justification for the layered description used in Figure 6a, b to draw an analogy to the $CaCu_5$ type. In CP plots of Figure 7d, e we emphasize the same layers in these environments using thicker cylinders. The contacts within the layers on the whole exhibit different CP features than those between them: the intralayer contacts tend to be punctuated with positive pressure lobes, whereas many of those between the layers show negative CP. These layers that were originally identified in a search for connections to the $CaCu_5$ type thus have some relevance to the electronic structure of the phase.

In summary, the $Ca_{14}Cd_{51}$ structure can be seen as a more drastic response to the internal stresses of the $CaCu_5$ type than the Ca_2Ag_7 structure. In both cases, the deletion of transition metal atoms from the $CaCu_5$ type relieves negative CPs around the Ca atoms by providing tighter Ca coordination environments. In Ca_2Ag_7 the Ca coordination number by Ag is decreased from 18 to 14, whereas in $Ca_{14}Cd_{51}$ this number gets as low as 13 (for the Ca3 site). This, of course, suits the greater severity of the CP issues in $CaCd_5$ compared to its Ag analogue.

3.6. The Cd-rich Path to Chemical Pressure Relief: Tsai-type Cluster Formation in $CaCd_6$. The complex structures we have considered so far all involved the use of TM-poor stoichiometries to tighten the coordination environments of the Ca atoms. In the Ca−Cd system, a series of phases are also present on the Cd-rich side of the 1:5 stoichiometry: a Tsai-type icosahedral quasicrystal and two approximants to it. A look at the CP distributions in these compounds offers the potential to include quasicrystallinity as a possible expression of the structural plasticity of intermetallics.

To explore this possibility, let us focus on the simplest (and thus most amenable to electronic structure calculations) of these phases: the 1/1 Tsai-type approximant $CaCd_6$ (Figure 8). Its structure consists of body-centered cubic packing of spheroidal Tsai-type clusters, which are usually described in terms of concentric shells. The center of the cluster is occupied by a Cd tetrahedron (Figure 8a), which is orientationally disordered in the refined crystal structures (although an ordering transition has been noted at low temperatures).[31,62−64] We will lock these tetrahedra to one specific orientation for computational feasibility. This is surrounded by a Cd pentagonal dodecahedron (Figure 8b), which is in turn encapsulated in a Ca icosahedron (Figure 8c), Cd icosidodecahedron (Figure 8d), and finally a defect soccer-ball arrangement of Cd atoms (Figure 8e).

From this point of view, this arrangement of atoms might appear to have little in common with the simple $CaCu_5$ type. However, if we zoom in on the Ca coordination polyhedron of $CaCd_6$, a connection begins to take shape (Figure 8g). The Ca sits in a pentagonal void space, defined by three staggered pentagons: one in the plane of the Ca, with the others above and below, an arrangement very similar to the double hexagonal antiprism that defines the Ca coordination environment in the $CaCu_5$ type (Figure 8h). In essence, the Ca's coordination in $CaCd_6$ is a pentagonal analog of that in the $CaCu_5$ type.

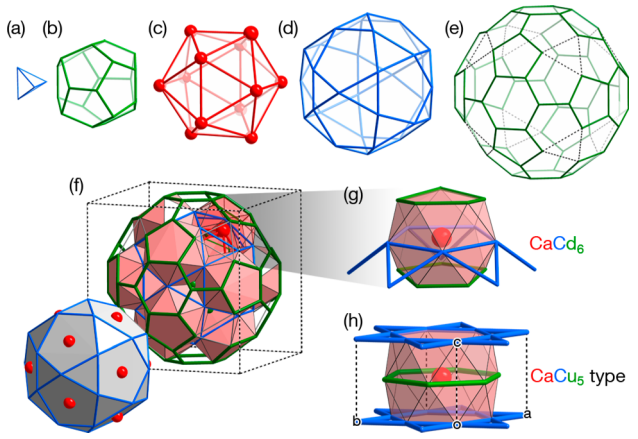

Figure 8. The quasicrystal approximant $CaCd_6$ is based on the Tsai-type cluster, which is usually described in terms of concentric polyhedra: (a) a central, positionally disordered Cd tetrahedron, (b) a Cd dodecahedron, (c) a Ca icosahedron, (d) a Cd icosidodecahedron, and (e) a defect Cd fullerene-like cage. The cluster packs in a body centered cubic fashion to form the full (f) $CaCd_6$ structure. A closer look at the (g) Ca coordination environment within this structure reveals a connection to (h) that in the $CaCu_5$ type.

The contraction from a hexagonal polyhedron to a pentagonal one would seem like an excellent means of relieving the negative CPs that would be experienced by the Ca atoms in the $CaCu_5$ type. Such is confirmed by a comparison of the CP distributions calculated for $CaCd_5$ and an ordered model of $CaCd_6$ (Figure 9). On moving from $CaCd_5$ to $CaCd_6$, the most intense Ca net negative CP features shrink significantly from

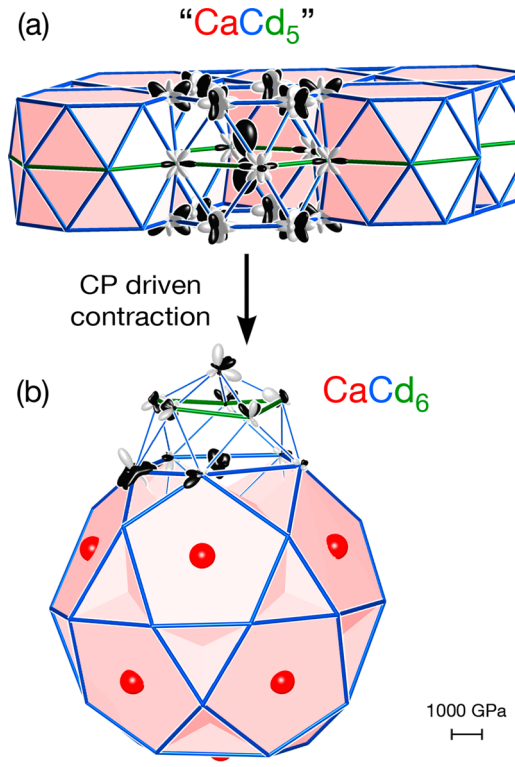

Figure 9. Chemical pressure-driven transition between the (a) hypothetical $CaCu_5$-type $CaCd_5$ and (b) the Tsai-type approximant $CaCd_6$. For plotting conventions, see the caption to Figure 2.

dx.doi.org/10.1021/ic5020412 | Inorg. Chem. 2014, 53, 10762−10771

−1253 GPa to −697 GPa, with the distribution of pressure lobes becoming much more isotropic.[65]

The use of pentagonal polyhedra thus helps satisfy the Ca atoms' need for tighter coordination, but it introduces a new problem: pentagonal units are significantly more difficult to arrange periodically in space than hexagonal ones. A beautiful solution to this issue is found by the structure of $CaCd_6$, as is detailed in our earlier communication:[22] the substitution of hexagons with pentagons is accommodated by the introduction of curvature. The shells of the Tsai-type cluster comprise curved analogues to the layers of the $CaCu_5$ type, in the same way as introducing pentagons into a graphene layer eventually leads to a C_{60} fullerene.

The relief of the CPs upon adopting the $CaCd_6$ structure extends beyond the Ca atoms' immediate surroundings. Most of the Tsai-type cluster from the icosidodecahedron down toward the core exhibits only relatively subtle CP features. The main exception is in some of the contacts between the central tetrahedron to the next shell outward, which may be partially relieved by moving to a model in which the orientations of these units are allowed to vary, providing a closer approximation to the true disorder. The largely strain-free nature of the cluster interior helps us understand why this unit should be the fundamental building block of Tsai-type quasicrystals.

All this is not to say, however, that the $CaCd_6$ structure is free from chemical pressures. If we shift our attention from the contents of the Tsai-type clusters to their interactions with each other, more intense pressure lobes become apparent. The strongest of these appear quite prominently at the unit cell faces where neighboring clusters meet through shared hexagons (see the Supporting Information for figures illustrating this). Such CP features at the cluster interfaces hint that alternative arrangements of the clusters may be favorable, as are indeed seen in the more complex $Ca_{13}Cd_{76}$ approximant,[44] and the $CaCd_{5.7}$ quasicrystal itself.[43,66]

Now that we have examined the CP scheme for $CaCd_6$, let us zoom out and compare the structural means of CP relief here with those of the Ca_2Ag_7 and $Ca_{14}Cd_{51}$ structures. In the structures we discussed earlier, the tighter Ca coordination environments were obtained by moving to a more Ca-rich stoichiometry: the removal of TM atoms led to fewer available for coordination to the Ca. In $CaCd_6$, the stoichiometry moves the other way, i.e. to the Cd-rich side of the 1:5 composition. Smaller Ca coordination environments here are achieved by using extra Cd atoms to reduce the sharing of these atoms by Ca coordination polyhedra. In the $CaCu_5$-type, the transition metals have either three or four Ca neighbors. In $CaCd_6$, the introduction of the Cd_4 tetrahedron at the Tsai-type cluster core and the absence of Ca atoms associated with the hexagons of the fullerene cage lowers the average number of Ca−Cd contacts per Cd to 2.72. Ca−Cd contacts are then given more freedom to contract in response to negative CP without the burden of stretching other Ca−Cd interactions.

4. CONCLUSIONS

In this Article, we have developed the theme of structural plasticity by combining updated results of our earlier DFT-CP studies of the Ca_2Ag_7 and $CaCd_6$ structures, with a new analysis of driving forces stabilizing the complex structure of $Ca_{14}Cd_{51}$. All three of these phases share a common origin in the presence of large negative CPs in the Ca coordination environments of the $CaCu_5$-type phase that would normally be anticipated to form in the Ca−Ag and Ca−Cd phases at the 1:5 stoichiometry. In each case, structural variations are introduced which tighten the Ca coordination, but different approaches are taken to accomplish this. In Ca_2Ag_7 and $Ca_{14}Cd_{51}$, the $CaCu_5$ type is progressively fragmented through the deletion of Ag/Cd atoms. In $CaCd_6$, however, additional Cd atoms are incorporated to create greater independence of the Ca coordination polyhedra. The ability of the structures to choose between transition metal insertion and deletion to modulate the surroundings of the Ca atoms is represented by the two branches of the structural family tree in Figure 1.

Through this work, we have seen how the concept of structural plasticity can be used to draw causal relationships among a disparate collection of crystal structures. We are looking forward to further expanding this network of connections, and to exploring how this concept can be applying to a broader range of solid state inorganic compounds. In terms of building on model system described in this Article, the $AuBe_5$ structure type is another common crystal structure that is adopted by compounds that combine late transition metals with an electropositive metal. We recently illustrated how its stability relative to the $CaCu_5$ type is enhanced as the electropositive metal is made smaller.[19] The transition from the $CaCu_5$ to $AuBe_5$ types could be added as a fixed stoichiometry branch to Figure 1, with the $AuBe_5$ type then serving as the starting point for the complex $AuBe_5$−$MgCu_2$ intergrowth structures that have been observed in compounds such as $YbCu_{4.5}$ (*mC*7448).[67,68]

Another potential use of the structural relationships revealed in this work is the design of syntheses targeting new phases. As all of the complex structures discussed here emerge from the release of negative pressures around the Ca sites in $CaCu_5$-type phases, elemental substitutions that modulate these pressures could be used to stabilize other structures. For instance, the partial replacement of Cd or Ag in the Ca−Cd and Ca−Ag systems, respectively, with smaller Pd atoms would lessen the stresses in the Ca coordination environments. This in turn could lead an enhancement of the $CaCu_5$-type features with new distributions of interfaces in the reaction products. An exciting avenue for future research will be to explore these expectations through solid-state synthesis.

■ ASSOCIATED CONTENT

Supporting Information

Details of the parameters used in the electronic structure calculations; LDA-DFT optimized atomic coordinates for the phases discussed, with total energies; additional discussion and illustrations of (1) the atomic packing in the intercolumnar matrix of the $Ca_{14}Cd_{51}$ structure, and (2) the CP scheme of the Tsai type cluster and cluster interfaces in $CaCd_6$. This material is available free of charge via the Internet at http://pubs.acs.org.

■ AUTHOR INFORMATION

Corresponding Author

*E-mail: danny@chem.wisc.edu.

Notes

The authors declare no competing financial interest.

■ ACKNOWLEDGMENTS

We thank Joshua Engelkemier and Yiming Guo for helpful conversations contributing to this work. We also are grateful to the National Science Foundation for financial support through

Grant DMR-1207409. This work utilized computer resources supported by NSF grant CHE-084494.

REFERENCES

(1) Barlow, C. Y.; Hansen, N. In *Materials Processing Handbook*; Groza, J. R., Shackelford, J. F., Lavernia, E. J., Powers, M. T., Eds.; CRC Press LLC: Boca Raton, FL, 2007; pp 12/13−12/29.
(2) Wang, Y.; Chen, M.; Zhou, F.; Ma, E. *Nature* **2002**, *419*, 912−915.
(3) Jin, H.-J.; Weissmüller, J. *Science* **2011**, *332*, 1179−1182.
(4) Koga, T.; Cronin, S. B.; Dresselhaus, M. S.; Liu, J. L.; Wang, K. L. *Appl. Phys. Lett.* **2000**, *77*, 1490−1492.
(5) Venkatasubramanian, R.; Siivola, E.; Colpitts, T.; O'Quinn, B. *Nature* **2001**, *413*, 597−602.
(6) Higgins, J. M.; Schmitt, A. L.; Guzei, I. A.; Jin, S. *J. Am. Chem. Soc.* **2008**, *130*, 16086−16094.
(7) Snyder, G. J.; Toberer, E. S. *Nat. Mater.* **2008**, *7*, 105−114.
(8) Poudeu, P. F. P.; Guéguen, A.; Wu, C.-I.; Hogan, T.; Kanatzidis, M. G. *Chem. Mater.* **2009**, *22*, 1046−1053.
(9) Kovalenko, M. V.; Spokoyny, B.; Lee, J.-S.; Scheele, M.; Weber, A.; Perera, S.; Landry, D.; Talapin, D. V. *J. Am. Chem. Soc.* **2010**, *132*, 6686−6695.
(10) Sambles, R. *Nature* **2005**, *438*, 295−296.
(11) Grigorenko, A. N.; Geim, A. K.; Gleeson, H. F.; Zhang, Y.; Firsov, A. A.; Khrushchev, I. Y.; Petrovic, J. *Nature* **2005**, *438*, 335−338.
(12) Pearson, W. B. *The Crystal Chemistry and Physics of Metals and Alloys*; Wiley-Interscience: New York, 1972.
(13) Fredrickson, D. C.; Lee, S.; Hoffmann, R. *Angew. Chem., Int. Ed.* **2007**, *46*, 1958−1976.
(14) Schmidt, J. T.; Lee, S.; Fredrickson, D. C.; Conrad, M.; Sun, J. L.; Harbrecht, B. *Chem.—Eur. J.* **2007**, *13*, 1394−1410.
(15) Cenzual, K.; Parthé, E.; Waterstrat, R. M. *Acta Crystallogr., Sect. C* **1986**, *42*, 261−266.
(16) Yang, Q.-B.; Andersson, S.; Stenberg, L. *Acta Crystallogr., Sect. B* **1987**, *43*, 14−16.
(17) Fredrickson, D. C. *J. Am. Chem. Soc.* **2012**, *134*, 5991−5999.
(18) Engelkemier, J.; Berns, V. M.; Fredrickson, D. C. *J. Chem. Theory Comput.* **2013**, *9*, 3170−3180.
(19) Berns, V. M.; Engelkemier, J.; Guo, Y.; Kilduff, B. J.; Fredrickson, D. C. *J. Chem. Theory Comput.* **2014**, *10*, 3380−3392.
(20) Harris, N. A.; Hadler, A. B.; Fredrickson, D. C. *Z. Anorg. Allg. Chem.* **2011**, *637*, 1961−1974.
(21) Hadler, A. B.; Harris, N. A.; Fredrickson, D. C. *J. Am. Chem. Soc.* **2013**, *135*, 17369−17378.
(22) Berns, V. M.; Fredrickson, D. C. *Inorg. Chem.* **2013**, *52*, 12875−12877.
(23) Fulfer, B. W.; McAlpin, J. D.; Engelkemier, J.; McCandless, G. T.; Prestigiacomo, J.; Stadler, S.; Fredrickson, D. C.; Chan, J. Y. *Chem. Mater.* **2014**, *26*, 1170−1179.
(24) Fredrickson, D. C. *J. Am. Chem. Soc.* **2011**, *133*, 10070−10073.
(25) Palenzona, A. *J. Less Common Met.* **1970**, *21*, 443−446.
(26) Cordier, G.; Henseleit, R. *Z. Kristallogr.* **1991**, *194*, 146.
(27) Snyder, G. J.; Simon, A. *J. Alloys Compd.* **1995**, *223*, 65−69.
(28) McMasters, O. D.; Gschneider, K. A., Jnr.; Venteicher, R. F. *Acta Crystallogr. B* **1970**, *26*, 1224−1229.
(29) Bruzzone, G. *Gazz. Chim. Ital.* **1972**, *102*, 234−242.
(30) Larson, A. C.; Cromer, D. T. *Acta Crystallogr., Sect. B* **1971**, *27*, 1875−1879.
(31) Gómez, C. P.; Lidin, S. *Phys. Rev. B* **2003**, *68*, 024203.
(32) Gonze, X.; Rignanese, G.-m.; Verstraete, M.; Beuken, J.-m.; Pouillon, Y.; Caracas, R.; Raty, J.-y.; Olevano, V.; Bruneval, F.; Reining, L.; Godby, R.; Onida, G.; Hamann, D. R.; Allan, D. C. *Z. Kristallogr.* **2005**, *220*, 558−562.
(33) Gonze, X.; Amadon, B.; Anglade, P.-M.; Beuken, J.-M.; Bottin, F.; Boulanger, P.; Bruneval, F.; Caliste, D.; Caracas, R.; Côté, M.; Deutsch, T.; Genovese, L.; Ghosez, P.; Giantomassi, M.; Goedecker, S.; Hamann, D. R.; Hermet, P.; Jollet, F.; Jomard, G.; Leroux, S.; Mancini, M.; Mazevet, S.; Oliveira, M. J. T.; Onida, G.; Pouillon, Y.; Rangel, T.; Rignanese, G.-M.; Sangalli, D.; Shaltaf, R.; Torrent, M.; Verstraete, M. J.; Zerah, G.; Zwanziger, J. W. *Comput. Phys. Commun.* **2009**, *180*, 2582−2615.
(34) Goedecker, S.; Teter, M.; Hutter, J. *Phys. Rev. B* **1996**, *54*, 1703−1710.
(35) Hartwigsen, C.; Goedecker, S.; Hutter, J. *Phys. Rev. B* **1998**, *58*, 3641−3662.
(36) The DFT-Chemical Pressure Package is freely available on our research group's homepage at URL: http://www.chem.wisc.edu/~danny/; last accessed: 31 Aug. 2014.
(37) Pearson, W. B. *Acta Crystallogr., Sect. B* **1968**, *24*, 1415−1422.
(38) Palenzona, A.; Manfrinetti, P. *J. Less Common Met.* **1982**, *85*, 307−312.
(39) Subramanian, P. R. In *Binary Alloy Phase Diagrams*, 2nd ed.; Massalski, T. B., Ed.; ASM International: Materials Park, OH, 1990; Vol. *44*, pp 899−901.
(40) We give numerical values for the pressures to help make the CP plots more tangible, but with the recognition that the quantitative values are dependent on such factors as the pseudopotentials used in the DFT calculation and the details of the integration scheme employed for interpretting the CP maps. More important than the numerical values are the relative sizes of the CP features for the various interactions, and the degree to which they can be relieved through structural transformations.
(41) In this discussion, we focus more on changes in the relative sizes of the CP features on replacing Pd with Ag or Cd than on changes in the numerical values for the pressures. In our previous work using CP analyses, we found that comparisons between the CP magnitudes for systems with different elements are made difficult by the differences in the electronic structures of the component atoms.
(42) Kleber, W. *Krist. Technik* **1967**, *2*, 13−14.
(43) Guo, J.; Abe, E.; Tsai, A. P. *Phys. Rev. B* **2000**, *62*, R14605−R14608.
(44) Gómez, C. P.; Lidin, S. *Angew. Chem., Int. Ed.* **2001**, *40*, 4037−4039.
(45) Bailey, D. M.; Kline, G. R. *Acta Crystallogr., Sect. B* **1971**, *27*, 650−653.
(46) Gabathuler, J.-P.; White, P.; Parthé, E. *Acta Crystallogr., Sect. B* **1975**, *31*, 608−610.
(47) Allibert, C.; Wong-Ng, W.; Nyburg, S. C. *Acta Crystallogr., Sect. C* **1984**, *40*, 211−214.
(48) Palenzona, A.; Cirafici, S. *J. Less Common Met.* **1986**, *124*, 245−249.
(49) Cirafici, S.; Palenzona, A. *J. Less Common Met.* **1987**, *135*, 1−4.
(50) Dommann, A.; Hulliger, F. *J. Less Common Met.* **1988**, *141*, 261−273.
(51) Palenzona, A.; Cirafici, S. *J. Less Common Met.* **1988**, *143*, 167−171.
(52) Dommann, A.; Ott, H. R.; Hulliger, F.; Fischer, P. *J. Less Common Met.* **1990**, *160*, 171−180.
(53) Canepa, F.; Palenzona, A.; Eggenhöffner, R. *Physica B* **1992**, *176*, 293−300.
(54) Saccone, A.; Fornasini, M. L.; Macciò, D.; Delfino, S. *Intermetallics* **1996**, *4*, 111−119.
(55) Saccone, A.; Macciò, D.; Giovannini, M.; Delfino, S. *J. Alloys Compd.* **1997**, *247*, 134−140.
(56) Saccone, A.; Macciò, D.; Delfino, S.; Ferro, R. *Intermetallics* **2000**, *8*, 229−237.
(57) Gumenyuk, R.; Kuz'ma, Y. *Inorg. Mater.* **2007**, *43*, 135−137.
(58) Belgacem, B.; Pasturel, M.; Tougait, O.; Potel, M.; Roisnel, T.; Ben Hassen, R.; Noël, H. *J. Alloys Compd.* **2009**, *478*, 89−95.
(59) Lin, Q.; Corbett, J. D. *Inorg. Chem.* **2011**, *50*, 1808−1815.
(60) Verbovytskyy, Y.; Gonçalves, A. P. *Intermetallics* **2013**, *33*, 16−26.
(61) Tkachuk, A. V.; Mar, A. *Inorg. Chem.* **2008**, *47*, 1313−1318.
(62) Ryuji, T.; Yohsuke, M.; Shin, T.; Masaki, I.; Masahiko, I.; Yutaka, U. *Jpn. J. Appl. Phys.* **2002**, *41*, L524.
(63) Widom, M.; Mihalkovič, M. *MRS Online Proc. Libr.* **2003**, *805*, LL1.10.

(64) Tamura, R.; Edagawa, K.; Murao, Y.; Takeuchi, S.; Suzuki, K.; Ichihara, M.; Isobe, M.; Ueda, Y. *J. Non-Cryst. Solids* **2004**, *334*−*335*, 173−176.
(65) When we add this observation of CP reduction in $CaCd_6$ to our similar result for $Ca_{14}Cd_{51}$, we can tentatively draw some conclusions about the thermodynamic instability of a hypothetical $CaCd_5$ phase relative to decomposition into a two-phase mixture as in $CaCd_5 \rightarrow (1-x)CaCd_6 + xCaCd_{3.643}$ (= $Ca_{14}Cd_{51}/14$), with $x = 0.4242$ (or a similar reaction involving the more complicated Tsai-cluster based phases). In this balanced equation, one phase with large negative pressures on the Ca atoms reacts to form a Cd-rich and Cd-poor phase, both of which have lower magnitude CP features on the Ca. If we were to envision similar energy vs distance curves between the phases for each type of interaction (Ca−Ca, Ca−Cd, Cd−Cd), then we could then make an argument about this being a thermodynamically favorable reaction. However, we prefer to emphasize the stabilization of local features in these structures.
(66) Takakura, H.; Gómez, C. P.; Yamamoto, A.; De Boissieu, M.; Tsai, A. P. *Nat. Mater.* **2007**, *6*, 58−63.
(67) Černý, R.; François, M.; Yvon, K.; Jaccard, D.; Walker, E.; Petříček, V.; Císařova, I.; Nissen, H.-U.; Wessicken, R. *J. Phys.: Condens. Matter* **1996**, 4485.
(68) Gottlieb-Schönmeyer, S.; Brühne, S.; Ritter, F.; Assmus, W.; Balanetskyy, S.; Feuerbacher, M.; Weber, T.; Steurer, W. *Intermetallics* **2009**, *17*, 6−10.